Science of the Total Environment 865 (2023) 161182

Contents lists available at ScienceDirect

Science of the Total Environment

journal homepage: www.elsevier.com/locate/scitotenv

Short communication

Macronutrients, iron and humic substances summer cycling over the extended continental shelf of the South Brazil Bight

Camila Fiaux Sukekava [a,b,*], Carlos Francisco Ferreira de Andrade [a], Luis Felipe Hax Niencheski [a], Marcio Silva de Souza [a], Luis M. Laglera [b]

[a] Instituto de Oceanografia, Fundação Universidade Federal do Rio Grande, Rio Grande 96203900, Brazil
[b] Departamento de Química, Universidad de las Islas Baleares, Palma, Balearic Islands 07122, Spain

HIGHLIGHTS

- Upwelling macronutrients at the shelf edge in SBB coast during NE wind episodes
- Iron ligand did not couple with dissolved iron concentrations.
- Non-humic ligands controlled surface Fe speciation.
- Iron-humic complexes important in upwelled waters
- Dust and sediment resuspension are iron sources in coastal SBB.

GRAPHICAL ABSTRACT

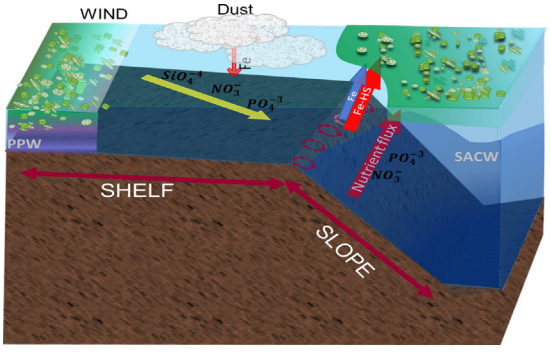

ARTICLE INFO

Editor: Julian Blasco

Keywords:
South Brazil Bight (SBB)
Upwelling
Macronutrients
iron speciation
Humic substances

ABSTRACT

We surveyed macronutrients and dissolved iron (DFe) concentrations and speciation in a transect over the shelf of the South Brazil Bight (SBB) at Santa Marta Grande Cape (SE Brazil) during a coastal downwelling episode. Driven by dominant NE winds, coastal downwelling is a common feature during the austral summer and force after water convergence, with contribution of internal wave breaking at the shelf edge, upwelling of macronutrients into the nutrient-depleted waters of the southbound Brazil Current at ~100 km from the coastline. As a result, we found a plume of high turbidity that reached the euphotic layer, a deepening of the silicate, nitrate, and phosphate isolines over the shelf and a bulging of the nitrate and phosphate isolines over the shelf edge and the slope. Our first measurements of DFe concentration and speciation in the area revealed that against prior findings in other coastal areas, macronutrients, DFe, and iron ligand cycles were disentangled. Higher DFe concentrations were often found at the surface indicating aerial deposition. Secondary DFe maxima over the sediment-water interface and in the upwelled plume indicated DFe fluxes from the sediment and from resuspended instable colloids. Iron ligand concentrations were higher than DFe concentrations in most stations with a clear land-to-ocean gradient. Subtraction of HS iron ligands revealed that except in upwelled water, the bulk of surface ligands was the result of local biological processes. The analysis of the concentrations of Fe-HS complexes showed that the contribution of HS to DFe was dominant in upwelled waters, significant in waters close to the coast, but nearly negligible in the rest of the studied area. We hypothesize that the injection of iron-humic complexes into the euphotic layer during summer upwelling episodes is the key to understanding the persistent high chlorophyll meanders found over the shelf edge of the SBB coast.

* Corresponding author at: Instituto de Oceanografia, Fundação Universidade Federal do Rio Grande, Rio Grande, Av Italia km 8, 96203900, Brazil.
E-mail address: camilasukekava@gmail.com (C.F. Sukekava).

http://dx.doi.org/10.1016/j.scitotenv.2022.161182
Received 23 September 2022; Received in revised form 10 December 2022; Accepted 21 December 2022
Available online xxxx

1. Introduction

The Santa Marta Grande (SMG) Cape is located on the Southeast coast of Brazil, in the southern section of the South Brazil Bight (SBB). The SBB starts in Rio de Janeiro (23°S) and ends in the Santa Catarina state (28.5°S). From an economic perspective, the SMG is a relevant fishing area and serves as a fish nursery for many species (Franco et al., 2020). The SBB shelf is remarkably wide with an average width of approximately 150 km (maximum of 230 km), whose edge is found at 150 to 185 m deep (Martins and Coutinho, 1981). The bathymetry at the SMG Cape is particularly characterized by a nearly flat shelf (declivity 1:300/600) and a shelf edge line located ~100 km from the coast, which is closer to the coast than in most of the SBB region. The SBB is an example of the poorly studied coastal systems defined by low terrestrial waters inputs and biogeochemical processes ruled by the effect of wind dynamics.

The oceanography of the SMG area presents a stratified water mass structure. Freshwater river discharge has a small contribution concealed to the inner shelf (Campos et al., 1995). The Brazilian Current (BC), the southbound split of the Atlantic South Equatorial Current after bifurcation off Cape São Roque (Stramma et al., 1990), which is defined by warm and high salinity waters, occupies the outer shelf edge. The BC is a relatively weak South Atlantic western boundary current that flows southwards as a shallow current (confined to the upper 500 m) carrying warm and saline tropical waters. It is composed of two water masses: the shallow Tropical Water (TW) and the deeper South Atlantic Central Water (SACW). TW transports low macronutrient concentrations, opposed to the high macronutrient concentrations found in the SACW (Braga et al., 2008; Niencheski et al., 2014; Piola et al., 2000). Seasonally changing wind dynamics force strong episodes of Ekman transport, with temporal episodes of combined coastal downwelling/shelf edge upwelling, and substantial changes of the SACW upper limit across the shelf during summer, the elevation of the SACW upper limit often reaches the euphotic layer. Winter freshwater inputs and summer upwelling pulses bring enough macronutrients to surface waters to increase biological productivity significantly of the otherwise macronutrient-depleted TW (Ciotti et al., 2014; Muelbert et al., 2008). Biogeochemical studies conducted in the SBB have revealed two major sources of macronutrients over the shelf and the slope with strong seasonal variations: continental exchanges and some upwelling pulses (Acha et al., 2004; Braga et al., 2008; Muelbert et al., 2008; Niencheski et al., 2014). Moreover, in restricted areas of strong bathymetry changes as shelf edges, the dissipation of internal waves generated by the effect of tidal currents over the topography may generate turbulence and localized macronutrients upward pulses (upwelling) (Cullen et al., 1983). This process has been verified in the outer shelf of the SE coast of Brazil with a peak during summers (Lorenzzetti and Dias, 2013).

Despite the oceanographic relevance of the SBB area, prior studies focused only on biological parameters and macronutrients (nitrate, silicate, phosphate) (Braga et al., 2008; Muelbert et al., 2008; Niencheski et al., 2014). To our knowledge, there are no reports in the area about the concentration and possible upwelling of micronutrients such as the essential element iron.

Iron is usually not limiting in coastal areas, although this has been questioned in the narrow shelf area of the Southern part of the California upwelling region for periods of low riverine inputs (Biller and Bruland, 2014; Bruland et al., 2001; Till et al., 2019). Iron uptake is key to primary productivity and the composition of the biological community (Geider and La Roche, 1994; Till et al., 2019). Iron is of relevance to CO_2 exchange between the atmosphere and the ocean in coastal areas (Ito et al., 2016). In shallow continental shelves, iron resuspension from sediments may be necessary for a substantial drawdown of upwelled nutrients by phytoplankton blooms (Capone and Hutchins, 2013).

The solubility of iron in seawater is extremely low (about 10^{-11} M in organic matter free seawater) due to the thermodynamical stability of the Fe (III) species, where inorganic speciation in seawater is dominated by the Fe $(OH)_3^0$ species (Liu and Millero, 2002). Low iron solubility limits its transition from continental waters into the open ocean. However, the presence of organic matter, and more specifically iron ligands, prevents iron precipitation resulting in dissolved iron concentrations on the coast (DFe) in the nanomolar range (Liu and Millero, 2002). The concentration of iron ligands and the conditional stability of their organic matter-DFe complex is routinely determined after competing ligand equilibrium and analysis by cathodic stripping voltammetry (CLE-CSV) in a set of sample aliquots titrated with DFe to which is added an artificial ligand for competition that forms an electroactive complex (Gerringa et al., 2014). Current research has proposed a short list of groups of organic substances as candidates to constitute the bulk of iron binding ligands in seawater: siderophores and their degradation products (Boiteau et al., 2016; Bundy et al., 2018; Mawji et al., 2008), pigments (Gledhill et al., 2013), polysaccharides (Hassler et al., 2011) and humic substances (HS) (Laglera and van den Berg, 2009). HS are the product of the biological and chemical transformations of terrestrial plant tissues and microbes that constitute a physical and chemical heterogeneous mixture of hydrophobic organics, ubiquitous in natural waters. In coastal waters, terrestrial-derived HS are expected to dominate iron complexation (Laglera and van den Berg, 2009), although there are doubts whether this effect, which is of major importance at high latitudes, is extended to lower latitudes (Krachler and Krachler, 2021).

Here, we present measurements of macronutrients and the micronutrient iron, including its organic speciation and the contribution of HS to DFe concentrations in a coast to ocean transect off the SMG cape. We sampled the water column over the whole shelf and the initial section of the slope during a coastal downwelling. Our aim was to determine the effect of such episodes in the distributions of macronutrients, DFe and HS. This study is the first to report iron concentrations and speciation on the SBB coast where the spatial distribution of nutrients and primary productivity are strongly controlled by intense wind variations.

2. Material and methods

2.1. Sampling

Water column samples were collected on board the RV Atlântico Sul in a transect perpendicular to the Southeast coast of Brazil at the Santa Marta Grande Cape (28.5°S) in January 2015 (summer) (Fig. 1). During the campaign, 22 samples were collected at six stations in one transect from the coast to the point of the slope where the sea bottom depth was 1500 m. Bottle closure depths were selected based on the vertical distribution of temperature and salinity to represent all the water masses present at the station. The deepest sample at each station was collected with the help of a pinger (SeaBird SBE19plus) at 5 m over the seafloor at stations 1 to 3 located over the shelf and at 10 m over the seafloor at stations 4 to 6 located over the shelf edge and the slope. Macronutrients and iron samples were collected using 12-liter Teflon-coated Go-Flo bottles suspended on a Kevlar line. The hydrographic data (CTD and dissolved oxygen) were collected using the SeaBird SBE9plus and SeaBird SBE19plus probes.

All samples for macronutrient analyses were filtered through 0.45 μm filters (cellulose acetate, Millipore®) immediately once onboard, with the help of a vacuum pump. Filtered samples destined to nitrate, phosphate, and silicate analyses were stored in polyethylene bottles, with chemicals added for analyte stabilization when needed, and then frozen pending later analysis. The analytical methodology is described in Strickland and Parsons (1972). A failure of the fluorescent probe after sampling the first two stations impeded the collection of fluorescence profiles thereafter. Instead, we used chlorophyll satellite images as a proxy for the distribution of primary producers at the surface. Chlorophyll concentrations were estimated using satellite images (https://www.star.nesdis.noaa.gov/socd/mecb/color/index.php).

Samples for DFe, organic iron speciation and humic substances analysis were immediately filtered by 0.2 μm cellulose nitrate membrane filters, (Millipore®) once onboard, stored in 250 mL low density polyethylene bottles and samples for analysis of DFe acidified to pH 2. Filters and bottles were treated before use according to standard GEOTRACES protocols

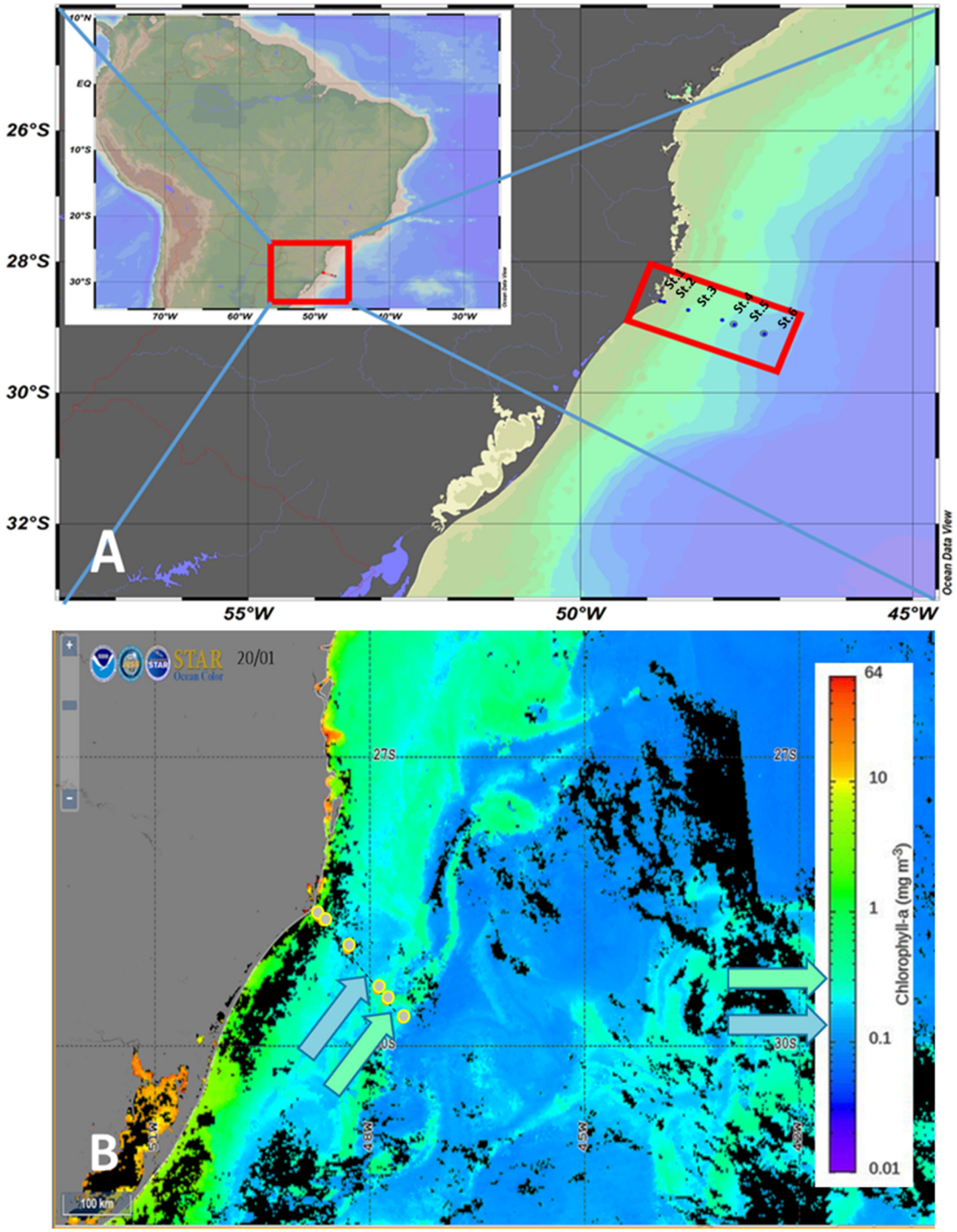

Fig. 1. (A) Map of the Southeast coast of Brazil showing the location of the transect sampled in this study, and name of each station. (B) Surface chlorophyll map of the studied area showing the sampled transect. The arrows point to two important features of the Brazilian Current, the intermediate area of lower biomass, and to the outer string of high biomass.

(Cutter et al., 2017) Speciation and HS samples were immediately frozen, and all analyses were carried out at the laboratories of the Federal University of Rio Grande.

2.2. Reagents

Water used for solution preparation and for rinsing containers was ultrapure (Milli-Q, Millipore®). A combined solution of Piperazine-*N,N′*-bis(2-hydroxypropanesulfonic acid) (POPSO, Sigma-Aldrich) and potassium bromate (Sigma-Aldrich) was prepared by using aqueous ammonia (Merck, Suprapur 40 %) at concentrations of 0.1 M and 0.4 M, respectively. The concentration of ammonia in this solution was such to set the pH at 8.2 if used for the determination of dissolved iron (Laglera et al., 2013) or 8.35, for the analysis of the concentration of HS and humic iron (Sukekava et al., 2018). A volume of 500 μL of this buffer/bromate solution was added to 10 mL of each sample. Trace element contamination in the buffer/bromate solution was removed by adding 100 μM suspended particulate MnO_2 which was removed after overnight equilibration (twice) by gravity filtration (0.2 μm acetate cellulose, Millipore®) (Laglera et al., 2007, 2013). For speciation studies, a buffer solution of POPSO (0.1

M) was prepared and cleaned of contamination with colloidal MnO_2 as described above. Procedural blanks were lower than 0.3 nM Fe per 500 μL addition of the combined bromate/POPSO solution and below the limit of detection for the POPSO and DHN solutions. A stock solution of 5 μM iron (III) was prepared from an atomic absorption spectrometry standard solution (1 ppm, BDH) with two dilution steps in acidified (HCl) ultrapure water (pH = 2.0). The 2,3-dihydroxynaphthalene (DHN, Merck) solution was prepared in pH 2 ultrapure water at a concentration of 10 mM. The Suwannee River fulvic acid (SRFA) standard (1S101F, International Humic Substances Society, IHSS) was prepared in Milli-Q water, at a concentration of 0.2 g L^{-1}. Before use, an aliquot of the SRFA standard solution was carefully saturated with the required concentration of iron to equal the binding capacity of the HS in ultrapure water (Sukekava et al., 2018) which was determined as described in Laglera et al. (2007).

2.3. Equipment

The voltammetric system consisted of an Autolab PS101T potentiostat (Ecochemie, Netherlands), connected to a voltammetric stand (Metrohm model 663VA) containing a hanging mercury drop electrode (HMDE), a glassy carbon rod counter electrode and a double junction, Ag/AgCl, reference electrode with a salt bridge filled with 3 M KCl. The instrument was controlled by NOVA 2.15 software (Metrohm). Samples (10 mL) were placed in a quartz voltammetric cell and stirred by a rotating PTFE rod.

2.4. Dissolved iron

DFe concentrations were determined after acidification (10 μL of 37 % HCl ultrapure) following a well-established CSV method in the presence of 30 μM DHN (Laglera et al., 2013) but adding a UV digestion step. Acidified samples were transferred to 30 mL quartz tubes and irradiated for 3 h using a home-built system including a 60 W high-pressure mercury vapor lamp. Before CSV analysis, the pH of samples was neutralized with ammonium (Merck, Suprapur 40 %) and the sensitivity was determined in every sample through internal additions of DFe. The accuracy of the analytical results was verified through replicate analyses certified seawater NASS-5 (National Research Council of Canada, NRC). We determined a concentration of 3.68 ± 0.14 nM, (n = 6), which was in excellent agreement with the certified value of 3.71 ± 0.63 nM. The detection limit (3σ of blank) was 0.024 nM.

2.5. Iron ligand concentrations and the stability constant of their complexes

Seawater samples (120 mL) were mixed in a Teflon bottle with DHN at a concentration of 1 μM and POPSO buffer at a concentration of 5 mM, respectively. Every sample was split into 12 aliquots of 10 mL to which iron was spiked in the range of 0 to 20 nM. The CLE-CSV method with DHN was described initially by van den Berg (2006), but was modified by removing the addition of bromate from the original method to avoid any underestimation of the contribution of HS to ligand concentrations (Laglera et al., 2011) and excluding the purge during the measurement (Caprara et al., 2015). All aliquots were equilibrated overnight at room temperature. The next day, each aliquot was spiked with 500 μL of the POPSO solution in order of increasing iron concentration and the concentration of the Fe-DHN complex determined by CSV analysis. The voltammetric parameters were as follows: a deposition potential of 0 V, adsorption time of 90 s, −5 mV of potential step with step intervals of 0.1 s and a potential scan using sample DC from −0.1 to −1.1 V.

Ligand concentrations and the conditional stability constants of their complexes with iron ($K'_{Fe'L}$) were obtained by fitting the CLE-CSV titration data into a linear Rûzic/van den Berg model, as described in Pižeta et al. (2015); Ružić (1982); van Den Berg (1982). Ligand concentrations are reported in nM and $K'_{Fe'L}$ values, reported in a logarithmic scale, and referred to the concentration of inorganic iron (Fe') as log $K'_{Fe'L}$.

2.6. Determination of humic substances and Fe-HS complexes

Samples were thawed and analyzed for HS concentrations and Fe-HS concentrations following established CSV procedures (Laglera et al., 2007; Sukekava et al., 2018). Briefly, the voltammetric method consisted in the deposition of Fe-HS complexes onto the HMDE at −0.1 V for 90 s before switching the potential to −1 V using DC sample at 50 mV s^{-1}, to force the reduction of adsorbed Fe(III)-HS complexes. The analysis included 3 steps: (1) measurement of HS concentrations in the samples, (2) saturation of the natural HS with added iron (20–60 nM depending on the magnitude of the initial signal), while monitoring the precipitation of excess dissolved iron until completion (marked by the stability of the Fe-HS CSV signal) and (3) determination of total HS using standard additions of a SRFA iron-saturated solution.

3. Results and discussion

3.1. Hydrography

Our area of study consists of a 100-km wide continental shelf and the adjacent slope influenced by many hydrographic features with strong seasonality (Campos et al., 2013; Piola et al., 2005). In general, high salinity and warm waters of the BC tend to separate from the coastal waters as the shelf widens. Samples were collected in a transect designed to cut perpendicularly the BC in its transit across the SMG Cape (Fig. 1). During fall and winter, SW winds are prevalent, and Plata Plume waters (PPW), characterized by low surface temperature (<18–20 °C) and salinity (<33.5), occupy the vicinity of the coast (Möller et al., 2008). However, during spring and summer, when NE winds are predominant, the PPW is retracted southwards and Itajaí River waters of low salinity and high temperature are found close to the coast (Campos et al., 2013). At the first few kilometers from the coast (stations 1 and 2) we found high temperature (>23 °C) and low salinity (<34.5) waters (Fig. 2), confirming the contribution of the Itajaí River to coastal waters (Campos et al., 2013).

Other distinctive local feature during the summer would be common wind-field variations that change the distribution of water masses alternating upwelling and downwelling pulses across the shelf depending whether NE or SE winds prevail (Campos et al., 2000, 2013). The depth of the 18.5 °C isotherm and the 35.3 PSU isohaline (upper boundary of the SACW) have been usually accepted as indicators of whether waters over the shelf are dominated by downwelling or upwelling periods at any given time during the summer (Campos et al., 2013; Ciotti et al., 2014). Since both isolines barely penetrated shelf waters (Fig. 2), the overall situation indicated downwelling in the first 70 km from the coastline. This was in line with the prevalent NE winds registered in the area during the 4 days prior to the sampling (Fig. S1). Coastal water downwelling forces by water convergence an upwelling of deep waters from the outer shelf (~100–120 km from the coast) to replace surface water close to the coast (Brandini et al., 2014; Campos et al., 2000). During our study, temperature and salinity isolines featured a domed shape at 100 km from the coastline, confirming water upwelling over the shelf edge (Fig. 2A and B). During strong episodes of upwelling, macronutrient-rich SACW waters can be injected into the euphotic layer (Brandini et al., 2014).

3.2. Other ancillary parameters

Oxygen concentrations showed a patchy pattern along the transect, albeit oxygen saturation showed a more coherent distribution. Local biogeochemical processes appeared to generate two major oxygen undersaturation sites: one near the coast in low salinity waters and another around the shelf edge region (Fig. 2C). Coastal oxygen undersaturation sites might result from the combination of intense respiration activity of grazers and large phytoplankton biomass (Ito et al., 2016).

The turbidity was high and nearly constant along the shelf and therefore across the salinity gradient that separated coastal freshwater inputs and TW

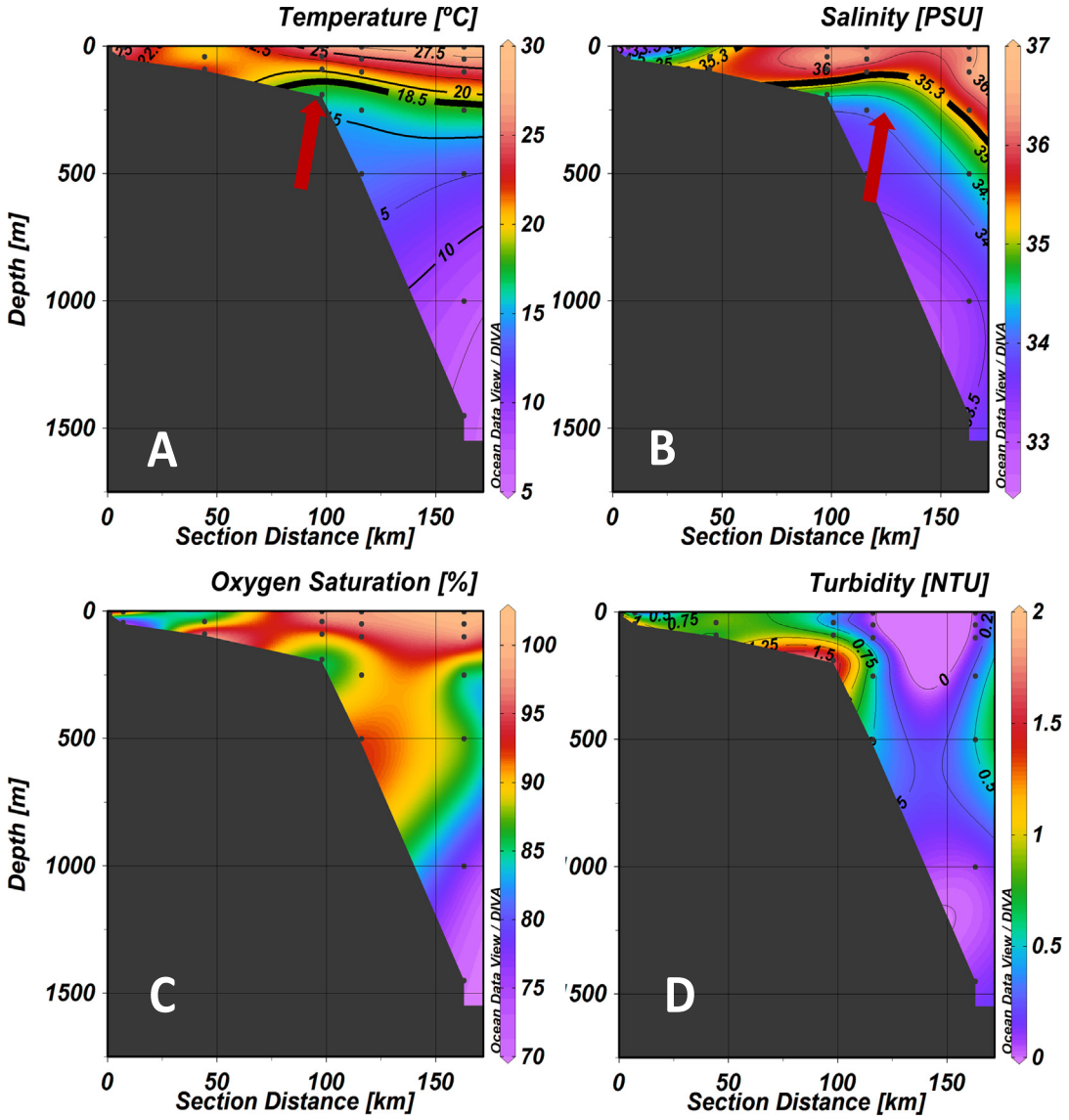

Fig. 2. Spatial distribution of temperature (°C) (A), salinity (PSU) (B), oxygen saturation (%) (C), and turbidity (NTU) (D) in the transect off the Santa Marta Grande cape. The arrows remark the dome shape of the 18.5 °C isotherm and the 35.3 °C isohel, upper limit of the South Atlantic Central Water (SACW), indicative of upwelling in the transition from shelf to slope.

(Fig. 2D). This lack of relationship with the salinity suggests a local resuspension of particles from the shelf sediments. At the shelf edge region, an area where water convergence and turbulence caused by the dissipation of internal waves combine to generate upwelling, there is a remarkable surge of turbidity (Fig. 2D). Our data indicate that the referred upwelling at the shelf edge was strong enough to bring along low oxygen interstitial waters with a high content in particles. For later comparison with chemical species measured in filtered samples, it is important to remark that turbidity is measured in unfiltered water and that light is not scattered below a particle size threshold.

Satellite pictures (Fig. 1B) show two maxima of chlorophyll-*a* concentrations along the transect which were related to the general distribution of biomass in the SBB region during our sampling. One along the first 20 km from the coastline (>2 mg·m^{-3}) and a secondary with moderate concentrations around the shelf edge (~0.35 mg·m^{-3}). Intermediate concentrations were below 0.14 mg m^{-3} (Fig. 1B). Over the studied area, this secondary maximum is generalized and appears in the satellite images as a high biomass meander separated from high biomass coastal waters by an area of low biomass area (Fig. 1B).

For the area that is very close to Santa Catarina State, concurrent relationships between the same oceanographic features described here and the spatial distribution of phytoplankton biomass were found. This coincidence suggests that the combination of shelf downwelling/slope upwelling and its repercussion in the formation of a secondary chlorophyll maximum at ~100 km from the coastline may be a generalized scenario in the region during the summer (Brandini et al., 2014).

3.3. Macronutrients

The BC is depleted in macronutrients although local coastal processes, such as the aforementioned freshwater discharge by rivers and wind-driven upwelling episodes, play a modulating role (Braga et al., 2008; Ciotti et al., 1995). Surface silicate concentrations were in the range of 2–18 μM (Fig. 3C). Previous studies have reported silicate concentration of 1–12 μM within SACW (Piola et al., 2000).

The three macronutrients correlated highly over the entire data set with Pearson correlations for nitrate vs phosphate and nitrate vs silicate of 0.804 ($p < 0.001$) and 0.710 ($p < 0.001$), respectively. This high correlation

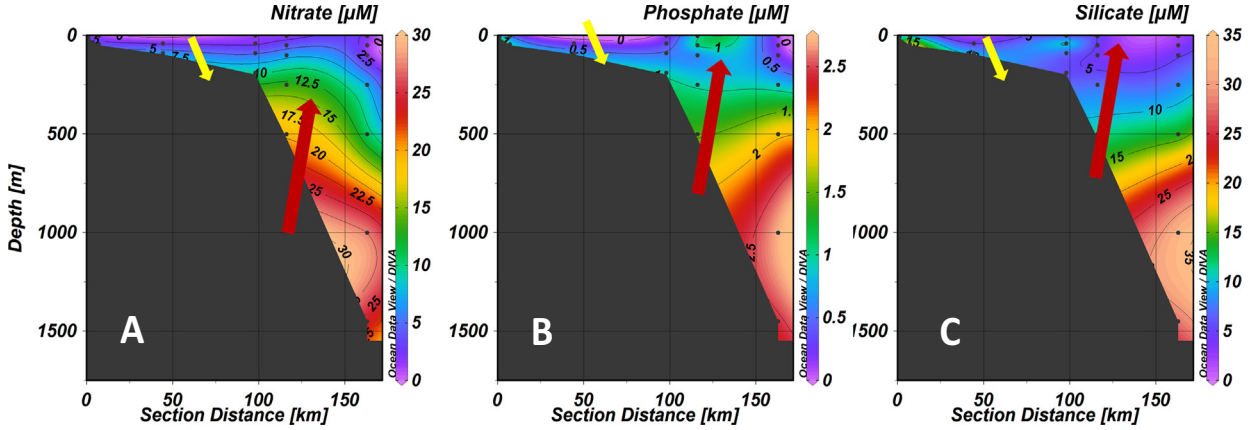

Fig. 3. Spatial distribution of nitrate (µM) (A), phosphate (µM), (B) and silicate (µM) (C) in the transect off Santa Marta Grande cape. Yellow arrows indicate location of the downwelling and red arrows location of upwelling.

indicates that macronutrient concentrations were probably the result of the same processes. The isolines of the three macronutrients sink and move away from the sea surface over the shelf whereas they showed a domed pattern over the shelf edge and beyond suggestive of upward transport. (Fig. 3). This scenario was in accordance with the referred coastal downwelling process leaving behind exhausted nutrient levels at the surface coupled to an upwelling of nutrient-rich upwelled waters near the shelf edge. Although it is difficult to estimate the exact contribution of this nitrate (and phosphate) input into the euphotic layer, it is safe to hypothesize that upwelling pulses contribute to form the high chlorophyll meander located at about 100 km from the coastline. Seawater N:P ratios were below the Redfield ratio of 16 in all but 3 samples. Fig. S2 shows that in the coastal downwelling area nitrogen was limiting but over the shelf edge, N:P ratios well over Redfield requirements formed a well-defined plume coincident with the turbidity maximum indicating nitrogen enrichment with respect to phosphate.

Silicate concentrations were minimum at the surface coincident with the chlorophyll maximum indicating that its surface distribution is modulated by primary productivity drawdown (Figs. 1B and 3C). There was no apparent upwelling of silicates at the shelf edge region (Fig. 3C). Since particles and other nutrients were substantially upwelled, we can suggest that sediments at that region were silica depleted.

3.4. Dissolved iron

In the studied area, DFe concentrations (all >0.9 nM) were one order of magnitude higher than what is considered limiting, so its role in controlling primary productivity was possibly not relevant (Fig. 4A). Fe:NO_3^- ratios in the upper 200 m over the area of study were in the range 0.17 to 4.2 nmol:µmol^{-1} and corroborated that nitrate was the limitant nutrient. These ratios are at least one order of magnitude higher than the ratios of 0.03 nmol:µmol^{-1} that mark the transition from nitrate to iron limitation in the California upwelling region (Biller and Bruland, 2014).

DFe concentrations also responded to the overall circulation pattern proposed and its isolines sank over the shelf and rose over the shelf edge in concomitance with nitrate, oxygen saturation, and turbidity data. However, over the slope, the trend was the opposite with higher DFe concentrations at the surface. Lower DFe concentrations at stations 1 and 2 with respect to station 3 can only be explained by a combination of low discharge of freshwater to the inner shelf area combined with enhanced, non-terrestrial iron inputs to the upper ocean in the outer shelf region. Aerial deposition, a common feature in the area, seems the most likely source of surface DFe for the first 60 km from the coast (Bif and Yunes, 2016). High DFe concentrations over the shelf edge and the slope sediments, point to an apparent resuspension of iron. On one hand, this is a regular situation in systems characterized by low oxygen saturation that favors the reduction of Fe(III) species into the highly soluble Fe(II) species. The reoxidation of Fe(II) back to Fe(III) as the oxygen saturation increases usually restricts this effect to the few first meters over the sediment. On the other hand, the DFe surge over the shelf edge is coupled with an increase of the turbidity, suggesting that colloidal and particulate iron is resuspended, with the consequent release of DFe by particulate/solution fluxes. It is difficult to measure the contribution of the two processes to the DFe plume located at the shelf edge. Since at stations 4 to 6 we found high DFe concentrations in all samples collected close to the bottom, the release of DFe (as Fe(II)) from the sediment seems to be a generalized feature. However, only the DFe plume associated to the maximum in turbidity is not confined to the vicinity of the sea floor and seems to make an impact in the euphotic layer. This indicates that particulate iron resuspension, possibly in the form of heterogeneous colloids, was an important feature at the sampling time. Turbidity decreased quickly from station 4 to 5 whereas the rest of chemical parameters affected by the upwelling advanced to station 5. We hypothesize that this decoupling of the distribution of turbidity and chemical species that seem related is caused by the progressive disaggregation of the resuspended particles. Particles, possibly a fraction of which were colloids formed by the interaction in pore waters of polynuclear iron nano-oxides with heterogeneous organic matter, were observed by turbidity but their content only partially analyzed because a significant fraction were too big to pass through our 0.2 µm filters. This mixed material has been observed in coastal plumes of peat-draining rivers (Muller and Cuscov, 2017). As these colloids penetrated more oxygenated and sunlit waters, they started to disaggregate and cancelled their contribution to the turbidity since became too small to scatter the light of the detector. However, downsizing promoted their incorporation to the filtrate, and increased their contribution to DFe concentrations. Surface DFe concentrations over 4 nM at Stations 5 and 6 (Fig. 4A) could be also explained by the aerial deposition referred above (Bif and Yunes, 2016). Finally, surface trophic biological processes may play a role in remineralizing part of the particulate iron (Laglera et al., 2017), since blooming surface waters influenced by upwelling of SACW waters, are characterized by high zooplankton biomass (Resgalla et al., 2001).

3.5. Iron speciation and the role of humic substances as iron ligands

To be able to extract the concentration of ligands and their $K'_{Fe'L}$, plotting of the fraction exchanged with an added ligand that forms an electroactive complex as a function of the iron added to the aliquot must show a characteristic curved shape. However, this is sometimes not the case in coastal waters (Sato et al., 2022; Su et al., 2016). This is often due to small ligand concentrations (equal or barely below DFe concentrations) of extremely high affinity and already saturated with iron, that interchange iron with the artificial ligand below the limit of detection. In two cases, the 40 m deep sample at station 3 and the bottom sample (190 m deep) at station 5, the linearity of the titration prevented the calculation of the ligand concentration and $K'_{Fe'L}$. In these two cases, and exclusively for studying DFe speciation, we decided to consider a ligand concentration equal to

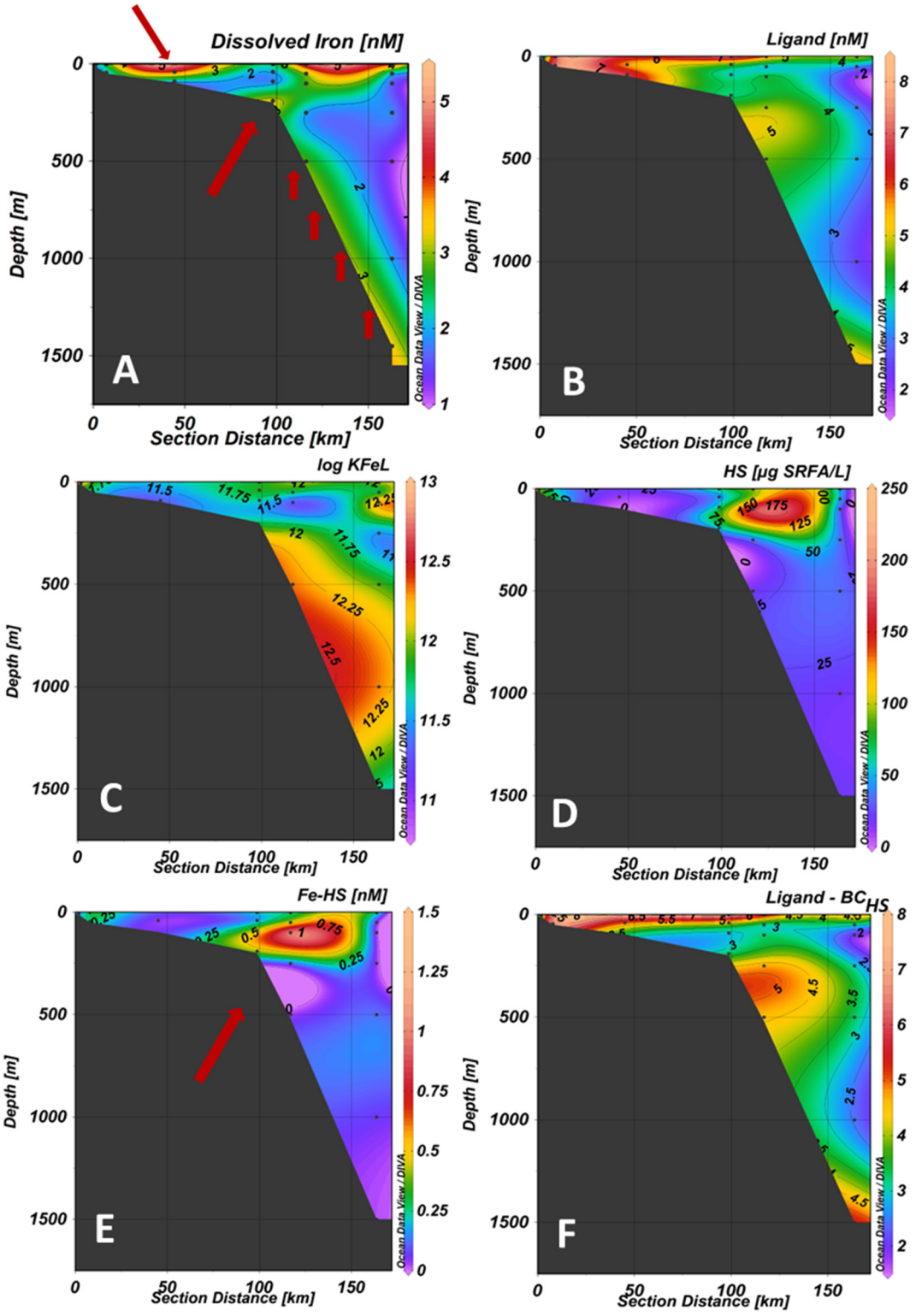

Fig. 4. Spatial Distribution of DFe (nM) (A), ligand (nM) (B), constant of stability (C), HS (µg SRFA L^{-1}) (D), Fe-HS (nM) (E) and overall ligands without the contribution of humic (F) in the transect off Santa Marta Grande cape. Yellow arrows indicate downwelling and red in the slope upwelling. The DFe plot had red arrow that show aerial deposition in surface and sediment resuspension.

the DFe concentration. This is based on the certainty that ligands were not absent in the sample. The extremely low solubility of inorganic iron requires complexation to maintain concentrations in solution in the nanomolar range. Ligand concentrations close to DFe concentrations were a common feature with ligand to DFe ratios lower than 2 in more than half the samples.

Along the shelf, ligand concentrations were high (2 to 8 nM) with a clear land to ocean gradient, with the highest values (~8 nM) found at the bottom of station 3 (Fig. 4B). This trend does not concur with the well-defined downwelling pattern shown by other variables. In contrast to DFe, ligands did not show high surface concentrations and did not seem to be upwelled at the shelf edge. To the best of our knowledge, the

decoupling of DFe and iron ligand concentrations in coastal waters has not been found before (Mellett et al., 2018; Su et al., 2015). Land to ocean ligand gradients usually indicate that terrigenous ligands, mainly composed of HS, could be the main source of ligands. However, HS were only high at stations 1 and 2 (60 to 110 μg SRFA L-1) and did not follow the horizontal gradient shown by overall ligands with some of the lowest HS concentrations found at station 3 (Fig. 4D). If we take the iron binding capacity of our SRFA standard, 14.6 ± 0.7 nmol Fe mg $SRFA^{-1}$, we can determine that the contribution of HS to ligand concentrations over the shelf was of 0.5 to 1.8 nM, which is only 10 to 20 % of the ligand concentrations (Table S1). The exception was station 1 and 2 where ligand concentrations were comprised of HS by 30 to 70 %. Our analytical scheme also included the determination of the contribution of Fe-HS complexes to the concentration of DFe. In waters over the shelf, HS binding sites with affinity for iron were found to be mostly iron-free with saturation indexes from 0 to 25 %, and Fe-HS concentrations were in the range below the limit of the detection (LOD, <0.03 nM) to 0.43 nM (Fig. 4E, Table S1). Therefore, the contribution of Fe-HS complexes to DFe over the shelf was in the range of ~0 to 25 %. This implies that despite the strong horizontal gradient of ligands and the vicinity to the coast, the contribution of HS to iron solubility over the shelf was low.

With respect to the other major area of interest, the shelf edge and the slope, ligand concentrations were also high except for station 6, which was less affected by water upwelling. At stations 4 and 5, ligand concentrations were in the range of 3 to 8 nM, while at station 6, ligand concentrations were in the range 2 to 5 (Fig. 4B). Since sediments accumulate a high concentration of decaying organic matter, and a part of it is expected to show affinity for iron, upwelling of interstitial waters must pump iron ligands into the water column. Ligand concentrations at the bottom of stations 5 and 6 were higher concurring with the DFe release from sediments shown above. However, this was not the case at station 4. In contrast, in the area affected by upwelled water at stations 4 and 5, HS concentrations were more than double than in surrounding waters (ranges of 30 to 240 and 20 to 40 μg SRFA L^{-1}, respectively) (Fig. 4D). This is the equivalent to ligand concentrations in the range 0.41 ± 0.04 to 3.5 ± 0.17 nM, which is equivalent to a contribution of HS to ligand concentrations ranging from 11 % to 68 % at the maximum HS concentration of 240 μg SRFA L^{-1} at 100 m deep at station 5 (Table S1). The origin of this HS input is clearly related to the upwelling of high-turbidity and nutrient-rich waters at the shelf edge, despite being the maximum HS concentration not found close to the bottom at station 4 (Fig. 4D). We hypothesize that the same disaggregation process mentioned in Section 3.4 was responsible of HS upwelling and explains the lack of correlation of turbidity with HS concentrations despite having a common origin. Another possible source of HS to the water column is the local degradation of the organic matter flux from the euphotic layer, in this case from the high chlorophyll meander. In the upwelled waters, concentrations of Fe-HS complexes up to 1.4 nM were substantial constituting up to 42 % of the DFe concentrations (100 m deep station 5) (Fig. 4E). Samples collected at station 6 and at station 5 below upwelled waters (including samples collected close to the slope bottom) showed a negligible contribution of HS to iron solubility (Fig. 4E).

Another approximation to the nature of the natural ligands can be inferred from the $K'_{Fe'L}$ values. However, there is one strong limitation since $K'_{Fe'L}$ values fall inside a range called "analytical window" determined by the concentration and stability of the complex formed by the added ligand and iron, i.e.: the ability to extract iron from the ligands found in the sample (Gerringa et al., 2014). In summary, too strong, and too weak ligands are not properly resolved. Weak ligands are fully outcompeted by the added ligand and left out of calculations. Iron complexes with strong ligands do not undergo ligand exchange after the addition of the added ligand, and although contribute to the ligand concentration, strong ligands do not weight in the determination of $K'_{Fe'L}$. Our analytical protocol set the center of our analytical window at a value in the lower end of the analytical windows used with different CLE-CSV methodologies to this date (side reaction coefficient or $\alpha'_{Fe'L}$ = [DHN] x $K'_{Fe'DHN}$ = 22.4) (Gerringa et al., 2021) with the aim to include the contribution of the weakest binding fraction of HS. In the whole area of study, log $K'_{Fe'L}$ values fell into the range of 10.9 to 12.9 (Fig. 4C). Overall, there is a clear depth interval (20 to 200 m) where ligands of lower stability (all <11.8) are found, mostly over the shelf. Stronger ligands (all >11.8) were found close to the coast, and at stations 4, 5 and 6 above and below the depth range referred to above including all samples collected close to the bottom of the slope (Fig. 4C). The traditional interpretation would point to a possible presence of HS in samples with lower log $K'_{Fe'L}$ based on previous reports that the affinity of HS for iron is about one order of magnitude lower than that of other natural ligands such as siderophores and porphyrins (Laglera and van den Berg, 2009; Witter et al., 2000). However, this is not the case here because of the lack of relation between the distributions of ligands, HS and log $K'_{Fe'L}$ (Fig. 4B and D). This same traditional approach shows that due to the high log $K'_{Fe'L}$ values found in surface waters, local biological production of ligands would be more important in the upper 20 m and below 200 m over the studied area. Theoretically, the use of an analytical window centered at a higher $\alpha'_{Fe'L}$ could have removed the contribution of weak ligands, many of HS nature, and become an arguable approach to resolve non humic ligands without our subtraction step. However, shifting of the CLE-CSV analytical window for iron speciation has been barely tested because the flexibility of many CLE-CSV methods to reduce or increase the concentration of the artificial ligand is very limited or require huge side corrections due to the presence of non-electroactive Fe-artificial ligand species (Mahmood et al., 2015) and the combined use of different artificial ligands has recently shown drawbacks (Gerringa et al., 2021). Moreover, the use of a higher analytical window could reduce the number of reliable results since out competition of weak ligands increases the possibility to obtain straight titrations like the two cases reported above.

Here we present for the first time a way to clarify the origin of ligands via the subtraction of the contribution of HS to iron speciation. Fig. 4F shows that once the contribution of HS to ligand concentrations is removed, the color plot of ligand distribution becomes more coherent. In the upper 200 m over the whole transect, non-humic ligands show a clear gradient from coast to open waters and from surface to bottom. Since high surface ligand concentrations extended well beyond the area of coastal influence, biological production (exudation or cellular lysis) must be the main source of non-humic ligands in the upper 200 m. Bottom samples at stations 5 and 6 also showed higher non-humic ligand concentrations, probably indicative of sediment release or bacterial remineralization (Burdige et al., 2004).

Fig. 4E shows that there are two areas of significant contribution of Fe-HS complexes to DFe concentrations: close to the coast and in upwelled waters. Apart from their iron binding ability, HS are characterized by their photolability and promote Fe reduction which increases substantially in the bioavailability of iron (Chen and Wang, 2008; Lis et al., 2015). The upwelling of DFe into the euphotic layer in the form of Fe-HS complexes probably increases its bioavailability with respect to other areas where other iron species are predominant (Muller, 2018). At the sediment-water interface of these two areas, DFe and ligand concentrations were high, and HS were absent, indicating that in sediments not affected by the upwelling, HS were either not present or, due to their size and/or chemical properties, remained in the interstitial waters. Only when the physical force at the water-sediment interface is strong enough to resuspend particles, are Fe-HS complexes a substantial contributor to upwelled DFe concentrations.

4. Conclusions

We observed upwelling of macronutrients and DFe over the shelf edge at 100 km from the coast as a response to NE summer wind regimes and turbulence generated by the dissipation of internal waves on the shelf edge. Our data do not allow us to estimate which one of the two processes controlled upwelling. Macronutrient injection reaching the euphotic layer helps to explain the discontinuity in coastal chlorophyll concentration and the formation of high biomass meanders parallel to the coast.

Surprisingly, DFe and iron ligands distributions were uncoupled with strong vertical gradients of DFe, suggesting aerial deposition, and a strong horizontal gradient of ligands. Uncoupling of HS and overall ligands

showed that most of surface ligands were of local biological origin although further investigation would be required to study the sources and fate of such ligands. DFe and ligands were also high in nearly all the stations where we collected samples close to the bottom, suggesting sediment to water column fluxes.

We detected an important source of Fe-HS complexes, clearly related to the upwelling of high-turbidity nutrient-rich waters over the shelf edge, that were stable enough to reach the euphotic layer at the shelf edge, and that contributed significantly to iron solubility. We conclude that high dissolved Fe-HS concentrations could be caused by disaggregation and dissolution of resuspended colloidal material of sedimentary origin. Future research to understand micronutrient dynamics should focus on the study of the composition and stability of particles upwelled from the outer section of continental shelves. The use of advanced methods to disentangle the contribution of HS to iron speciation from the rest of the binding components of DOM show that the contribution of HS to iron dynamics in the SMG is concealed to upwelling areas due to the low input of freshwater and the absence of dissolved HS fluxes from sediment to water.

CRediT authorship contribution statement

Camila Fiaux Sukekava: writing – original draft, formal analysis, conceptualization. **Carlo Francisco Ferreira de Andrade:** writing -review, resources. **Luis Felipe Hax Niencheski:** writing -review. **Marcio Silva de Souza:** writing -review, data curation. **Luis M. Laglera:** supervision, funding acquisition, visualization.

Data availability

Data will be made available on request.

Declaration of competing interest

The authors declare the following financial interests/personal relationships which may be considered as potential competing interests:

Luis M Laglera reports financial support was provided by the Spanish Government via the MINECO project (PID2020-115291GB-I00). Carlos F.F. de Andrade reports financial support was provided by MEC. CAMILA F. SUKEKAVA reports a relationship with Coordination of Higher Education Personnel Improvement that includes: funding grants. Marcio S. DE Souza reports a relationship with Coordination of Higher Education Personnel Improvement that includes: funding grants.

Acknowledgements

The authors wish to acknowledge all the people who helped in field sampling and analyses. We also thank the captain (Mr Homero) and the crew of R/V Atlântico Sul. Camila Sukekava participated in this work thanks to a grant provided by the Coordenação de Aperfeiçoamento de Pessoal de Nível Superior (CAPES). This research was financially supported by the Instituto Nacional de Ciência e Tecnologia em Ciências do Mar (INCT Mar-COI 565062/2010-7). M.S. de Souza is granted with a PNPD/MEC-CAPES fellowship number 88882.314596/2019-01. LML was supported by the project PID2020-115291GB-I00 funded by the MCIN/AEI/10.13039/501100011033.

Appendix A. Supplementary data

Supplementary data to this article can be found online at https://doi.org/10.1016/j.scitotenv.2022.161182.

References

Acha, E.M., Mianzan, H.W., Guerrero, R.A., Favero, M., Bava, J., 2004. Marine fronts at the continental shelves of austral South America: physical and ecological processes. J. Mar. Syst. 44, 83–105. https://doi.org/10.1016/j.jmarsys.2003.09.005.

Bif, M.B., Yunes, J.S., 2016. Distribution of the marine cyanobacteria trichodesmium and their association with iron-rich particles in the South Atlantic Ocean. Aquat. Microb. Ecol. 78, 107–119. https://doi.org/10.3354/ame01810.

Biller, D.V., Bruland, K.W., 2014. The Central California current transition zone: a broad region exhibiting evidence for iron limitation. Prog. Oceanogr. 120, 370–382. https://doi.org/10.1016/j.pocean.2013.11.002.

Boiteau, R.M., Mende, D.R., Hawco, N.J., McIlvin, M.R., Fitzsimmons, J.N., Saito, M.A., Sedwick, P.N., Delong, E.F., Repeta, D.J., 2016. Siderophore-based microbial adaptations to iron scarcity across the eastern Pacific Ocean. Proc. Natl. Acad. Sci. U. S. A. 113, 14237–14242. https://doi.org/10.1073/pnas.1608594113.

Braga, E.S., Chiozzini, V.C., Ucia Berbel, G.B., Maluf, J.C., Aguiar, V.M., Charo, M., Molina, D., Romero, S.I., Eichler, B.B., 2008. Nutrient Distributions Over the Southwestern South Atlantic Continental Shelf From Mar del Plata (Argentina) to Itajaí (Brazil): Winter-Summer Aspects. https://doi.org/10.1016/j.csr.2007.06.018.

Brandini, F.P., Nogueira, M., Simião, M., Carlos Ugaz Codina, J., Almeida Noernberg, M., 2014. Deep chlorophyll maximum and plankton community response to oceanic bottom intrusions on the continental shelf in the South Brazilian Bight. Cont. Shelf Res. 89, 61–75. https://doi.org/10.1016/j.csr.2013.08.002.

Bruland, K.W., Rue, E.L., Smith, G.J., 2001. Iron and macronutrients in California coastal upwelling regimes: implications for diatom blooms. Limnol. Oceanogr. 46, 1661–1674. https://doi.org/10.4319/LO.2001.46.7.1661.

Bundy, R.M., Boiteau, R.M., McLean, C., Turk-Kubo, K.A., McIlvin, M.R., Saito, M.A., Mooy, B.A.Van, Repeta, D.J., 2018. Distinct siderophores contribute to iron cycling in the mesopelagic at station ALOHA. Front. Mar. Sci., 1–15 https://doi.org/10.3389/fmars.2018.00061 in press.

Burdige, D.J., Kline, S.W., Chen, W., 2004. Fluorescent dissolved organic matter in marine sediment pore waters. Mar. Chem. 89, 289–311. https://doi.org/10.1016/j.marchem.2004.02.015.

Campos, E.J.D., Miller, J.L., Müller, T.J., Peterson, R.G., 1995. Physical oceanography of the Southwest Atlantic Ocean. Source Oceanogr. 8, 87–91.

Campos, E.J.D., Velhote, D., Da Silveira, I.C.A., 2000. Shelf break upwelling driven by Brazil current cyclonic meanders. Geophys. Res. Lett. 27, 751–754. https://doi.org/10.1029/1999GL010502.

Campos, P.C., Möller, O.O., Piola, A.R., Palma, E.D., 2013. Seasonal variability and coastal upwelling near Cape Santa Marta (Brazil). J. Geophys. Res. Oceans 118, 1420–1433. https://doi.org/10.1002/JGRC.20131.

Capone, D.G., Hutchins, D.A., 2013. Microbial biogeochemistry of coastal upwelling regimes in a changing ocean. Nat. Geosci. https://doi.org/10.1038/ngeo1916.

Caprara, S., Laglera, L.M., Monticelli, D., 2015. Ultrasensitive and fast voltammetric determination of iron in seawater by atmospheric oxygen catalysis in 500 μL samples. Anal. Chem. 87, 6357–6363. https://doi.org/10.1021/acs.analchem.5b01239.

Chen, M., Wang, W.X., 2008. Accelerated uptake by phytoplankton of iron bound to humic acids. Aquat. Biol. 3, 155–166. https://doi.org/10.3354/ab00064.

Ciotti, Á.M., Odebrecht, C., Fillmann, G., Moller, O.O., 1995. Freshwater outflow and subtropical convergence influence on phytoplankton biomass on the southern brazilian continental shelf. Cont. Shelf Res. 15, 1737–1756. https://doi.org/10.1016/0278-4343(94)00091-Z.

Ciotti, Á.M., de Mahiques, M., Möller, O.O., 2014. The meridional gradients of the S-SE brazilian continental shelf: introduction to the special volume. Cont. Shelf Res. 89, 1–4. https://doi.org/10.1016/j.csr.2014.08.008.

Cullen, J.J., Stewart, E., Renger, E., Eppley, R.W., Winant, C.D., 1983. Vertical motion of the thermocline, nitracline and chlorophyll maximum layers in relation to currents on the Southern California shelf (Ceratium). J. Mar. Res. 41, 239–262. https://doi.org/10.1357/002224083788520171.

Cutter, G.A., Casciotti, K., Croot, P.L., Geibert, W., Heimbürger, L.-E., Lohan, M., Planquette, H., van de Flierdt, T., 2017. Sampling and Sample-handling Protocols for GEOTRACES Cruises, Version 3. GEOTRACES Community Practices https://doi.org/10.25607/OBP-2.

Franco, B.C., Defeo, O., Piola, A.R., Barreiro, M., Yang, H., Ortega, L., Gianelli, I., Castello, J.P., Vera, C., Buratti, C., Pájaro, M., Pezzi, L.P., Möller, O.O., 2020. Climate change impacts on the atmospheric circulation, ocean, and fisheries in the southwest South Atlantic Ocean: a review. Clim. Change 162, 2359–2377. https://doi.org/10.1007/S10584-020-02783-6/FIGURES/5.

Geider, R.J., La Roche, J., 1994. The role of iron in phytoplankton photosynthesis, and the potential for iron-limitation of primary productivity in the sea. Photosynth. Res. 39, 275–301. https://doi.org/10.1007/BF00014588.

Gerringa, L.J.A., Rijkenberg, M.J.A., Thuróczy, C.E., Maas, L.R.M., 2014. A critical look at the calculation of the binding characteristics and concentration of iron complexing ligands in seawater with suggested improvements. Environ. Chem. 11, 114–136. https://doi.org/10.1071/EN13072.

Gerringa, L.J.A., Gledhill, M., Ardiningsih, I., Muntjewerf, N., Laglera, L.M., 2021. Comparing CLE-AdCSV applications using SA and TAC to determine the fe-binding characteristics of model ligands in seawater. Biogeosciences 18, 5265–5289. https://doi.org/10.5194/bg-18-5265-2021.

Gledhill, M., Achterberg, E.P., Honey, D.J., Nielsdottir, M.C., Rijkenberg, M.J.A., 2013. Distributions of particulate heme b in the Atlantic and southern oceans - implications for electron transport in phytoplankton. Glob. Biogeochem. Cycles 27, 1072–1082. https://doi.org/10.1002/2013GB004639.

Hassler, C.S., Schoemann, V., Nichols, C.M., Butler, E.C.V., Boyd, P.W., 2011. Saccharides enhance iron bioavailability to southern ocean phytoplankton. Proc. Natl. Acad. Sci. U. S. A. 108, 1076–1081. https://doi.org/10.1073/pnas.1010963108.

Ito, R.G., Garcia, C.A.E., Tavano, V.M., 2016. Net sea-air CO2 fluxes and modelled pCO2 in the southwestern subtropical Atlantic continental shelf during spring 2010 and summer 2011. Cont. Shelf Res. 119, 68–84. https://doi.org/10.1016/j.csr.2016.03.013.

Krachler, R., Krachler, R.F., 2021. Northern high-latitude organic soils as a vital source of river-borne dissolved iron to the ocean. Environ. Sci. Technol. 55, 9672–9690. https://doi.org/10.1021/acs.est.1c01439.

Laglera, L.M., van den Berg, C.M.G., 2009. Evidence for geochemical control of iron by humic substances in seawater. Limnol. Oceanogr. 54, 610–619. https://doi.org/10.4319/lo.2009.54.2.0610.

Laglera, L.M., Battaglia, G., Van den Berg, C.M.G., 2007. Determination of humic substances in natural waters by cathodic stripping voltammetry of their complexes with iron. Anal. Chim. Acta 599, 58–66. https://doi.org/10.1016/j.aca.2007.07.059.

Laglera, L.M., Battaglia, G., van den Berg, C.M.G., 2011. Effect of humic substances on the iron speciation in natural waters by CLE/CSV. Mar. Chem. 127, 134–143. https://doi.org/10.1016/j.marchem.2011.09.003.

Laglera, L.M., Santos-Echeandía, J., Caprara, S., Monticelli, D., 2013. Quantification of iron in seawater at the low picomolar range based on optimization of Bromate/Ammonia/Dihydroxynaphtalene system by catalytic adsorptive cathodic stripping voltammetry. Anal. Chem. 85, 2486–2492. https://doi.org/10.1021/ac303621q.

Laglera, L.M., Tovar-Sánchez, A., Iversen, M.H., González, H.E., Naik, H., Mangesh, G., Assmy, P., Klaas, C., Mazzocchi, M.G., Montresor, M., Naqvi, S.W.A., Smetacek, V., Wolf-Gladrow, D.A., 2017. Iron partitioning during LOHAFEX: copepod grazing as a major driver for iron recycling in the Southern Ocean. Mar. Chem. 196, 148–161. https://doi.org/10.1016/j.marchem.2017.08.011.

Lis, H., Shaked, Y., Kranzler, C., Keren, N., Morel, F.M.M., 2015. Iron bioavailability to phytoplankton: an empirical approach. ISME J. 9, 1003–1013. https://doi.org/10.1038/ismej.2014.199.

Liu, X., Millero, F.J., 2002. The solubility of iron in seawater. Mar. Chem. 77, 43–54. https://doi.org/10.1016/S0304-4203(01)00074-3.

Lorenzzetti, J.A., Dias, F.G., 2013. Internal solitary waves in the Brazilian SE continental shelf: observations by synthetic aperture radar. Int. J. Oceanogr. 2013, 1–11. https://doi.org/10.1155/2013/403259.

Mahmood, A., Abualhaija, M.M., van den Berg, C.M.G., Sander, S.G., 2015. Organic speciation of dissolved iron in estuarine and coastal waters at multiple analytical windows. Mar. Chem., 1–14 https://doi.org/10.1016/j.marchem.2015.11.001.

Martins, L.R., Coutinho, P.N., 1981. The Brazilian continental margin. Earth-Science Reviews 17, 87–107. https://doi.org/10.1016/0012-8252(81)90007-6.

Mawji, E., Gledhill, M., Milton, J.A., Tarran, G.A., Ussher, S., Thompson, A., Wolff, G.A., Worsfold, P.J., Achterberg, E.P., 2008. Hydroxamate siderophores: occurrence and importance in the Atlantic Ocean. Environ. Sci. Technol. 42, 8675–8680. https://doi.org/10.1021/es801884r.

Mellett, T., Brown, M.T., Chappell, P.D., Duckham, C., Fitzsimmons, J.N., Till, C.P., Sherrell, R.M., Maldonado, M.T., Buck, K.N., 2018. The biogeochemical cycling of iron, copper, nickel, cadmium, manganese, cobalt, lead, and scandium in a California current experimental study. Limnol. Oceanogr. 63, S425–S447. https://doi.org/10.1002/LNO.10751.

Möller, O.O.J., Piola, A.R., Cristina, A., Campos, E.J.D., 2008. The effects of river discharge and seasonal winds on the shelf off southeastern south. America 28, 1607–1624. https://doi.org/10.1016/j.csr.2008.03.012.

Muelbert, J.H., Acha, M., Mianzan, H., Guerrero, R., Reta, R., Braga, E.S., Garcia, V.M., Berasategui, A., Ramírez, F., Nica Gomez-Erache, M., 2008. Biological, Physical and Chemical Properties at the Subtropical Shelf Front Zone in the SW Atlantic Continental Shelf. https://doi.org/10.1016/j.csr.2007.08.011.

Muller, F.L.L., 2018. Exploring the potential role of terrestrially derived humic substances in the marine biogeochemistry of iron. Front. Earth Sci. 6, 1–20. https://doi.org/10.3389/feart.2018.00159.

Muller, F.L.L., Cuscov, M., 2017. Alteration of the copper-binding capacity of iron-rich humic colloids during transport from peatland to marine waters. Environ. Sci. Technol. 51, 3214–3222. https://doi.org/10.1021/acs.est.6b05303.

Niencheski, L.F., Windom, H.L., Moore, W.S., 2014. Controls on water column chemistry of the southern brazilian continental shelf. Cont. Shelf Res. 88, 126–139. https://doi.org/10.1016/j.csr.2014.07.007.

Piola, A.R., Campos, E.J.D., Möller, O.O., Charo, M., Martinez, C., 2000. Subtropical shelf front off eastern South America. J. Geophys. Res. Oceans 105, 6565–6578. https://doi.org/10.1029/1999JC000300.

Piola, A.R., Matano, R.P., Palma, E.D., Möller, O.O., Campos, E.J.D., 2005. The influence of the Plata River discharge on the western South Atlantic shelf. Geophys. Res. Lett. 32, 1–4. https://doi.org/10.1029/2004GL021638.

Pižeta, I., Sander, S.G., Hudson, R.J.M., Omanović, D., Baars, O., Barbeau, K.A., Buck, K.N., Bundy, R.M., Carrasco, G., Croot, P.L., Garnier, C., Gerringa, L.J.A., Gledhill, M., Hirose, K., Kondo, Y., Laglera, L.M., Nuester, J., Rijkenberg, M.J.A., Takeda, S., Twining, B.S., Wells, M., 2015. Interpretation of complexometric titration data: an intercomparison of methods for estimating models of trace metal complexation by natural organic ligands. Mar. Chem. 173, 3–24. https://doi.org/10.1016/j.marchem.2015.03.006.

Resgalla, C., De La Rocha, C., Montú, M., 2001. The influence of ekman transport on zooplankton biomass variability off southern Brazil. J. Plankton Res. 23, 641–650. https://doi.org/10.1093/PLANKT/23.6.641.

Ružić, I., 1982. Theoretical aspects of the direct titration of natural waters and its information yield for trace metal speciation. Anal. Chim. Acta 140, 99–113. https://doi.org/10.1016/S0003-2670(01)95456-X.

Sato, M., Wakuta, Y., Takeda, S., 2022. Distribution and chemical speciation of iron on the outer edge of the changjiang diluted water plume of the East China Sea. Cont. Shelf Res. 234. https://doi.org/10.1016/j.csr.2022.104646.

Stramma, L., Ikeda, Y., Peterson, R.G., 1990. Geostrophic transport in the Brazil current region north of 20°S. Deep Sea Res. Part A 37. https://doi.org/10.1016/0198-0149(90)90083-8.

Strickland, J.D.H., Parsons, T.R., 1972. A practical handbook of seawater analysis. 2nd editio. https://doi.org/10.25607/OBP-1791 Ottawa, Canada.

Su, H., Yang, R., Zhang, A., Li, Y., 2015. Dissolved iron distribution and organic complexation in the coastal waters of the East China Sea. Mar. Chem. 173, 208–221. https://doi.org/10.1016/j.marchem.2015.03.007.

Su, H., Yang, R., Pižeta, I., Omanovic, D., Wang, S., Li, Y., 2016. Distribution and speciation of dissolved iron in Jiaozhou Bay (Yellow Sea, China). Front. Mar. Sci. 3. https://doi.org/10.3389/fmars.2016.00099.

Sukekava, C., Downes, J., Slagter, H.A., Gerringa, L.J.A., Laglera, L.M., 2018. Determination of the contribution of humic substances to iron complexation in seawater by catalytic cathodic stripping voltammetry. Talanta 189, 359–364. https://doi.org/10.1016/j.talanta.2018.07.021.

Till, C.P., Solomon, J.R., Cohen, N.R., Lampe, R.H., Marchetti, A., Coale, T.H., Bruland, K.W., 2019. The iron limitation mosaic in the California current system: factors governing fe availability in the shelf/near-shelf region. Limnol. Oceanogr. 64, 109–123. https://doi.org/10.1002/LNO.11022.

van Den Berg, C.M.G., 1982. Determination of copper complexation with natural organic ligands in seawater by equilibration with MnO2 II. Experimental procedures and application to surface seawater. Mar. Chem. 11, 323–342. https://doi.org/10.1016/0304-4203(82)90029-9.

van den Berg, C.M.G., 2006. Chemical speciation of iron in seawater by cathodic stripping voltammetry with dihydroxynaphthalene. Anal. Chem. 78, 156–163. https://doi.org/10.1021/ac051441+.

Witter, A.E., Hutchins, D.A., Butler, A., Luther, G.W., 2000. Determination of conditional stability constants and kinetic constants for strong model fe-binding ligands in seawater. Mar. Chem. 69, 1–17. https://doi.org/10.1016/S0304-4203(99)00087-0.